ResearchGate

See discussions, stats, and author profiles for this publication at: https://www.researchgate.net/publication/305628945

# Noncontact Measurement of Complex Permittivity of Electrically Small Samples at Microwave Frequencies

**Article** *in* IEEE Transactions on Microwave Theory and Techniques · July 2016

DOI: 10.1109/TMTT.2016.2588487

CITATION
1

READS
82

**13 authors**, including:

Ying Wang
Anhui Agricultural University (AHAU)
**636** PUBLICATIONS **9,705** CITATIONS
SEE PROFILE

Dexin Ye
Zhejiang University
**37** PUBLICATIONS **335** CITATIONS
SEE PROFILE

Jiangtao Huangfu
Zhejiang University
**111** PUBLICATIONS **2,413** CITATIONS
SEE PROFILE

Changzhi Li
Texas Tech University
**214** PUBLICATIONS **2,200** CITATIONS
SEE PROFILE

**Some of the authors of this publication are also working on these related projects:**


KYSU Pawpaw Research Program View project


permittivity measurement, well logging View project

All content following this page was uploaded by Changzhi Li on 09 August 2016.

The user has requested enhancement of the downloaded file.

This article has been accepted for inclusion in a future issue of this journal. Content is final as presented, with the exception of pagination.



# Noncontact Measurement of Complex Permittivity of Electrically Small Samples at Microwave Frequencies

Jing Dong, Fazhong Shen, Yazhou Dong, Ying Wang, Wenli Fu, Huan Li, Dexin Ye, Bin Zhang, Jiangtao Huangfu, Shan Qiao, Yongzhi Sun, Changzhi Li, *Senior Member, IEEE*, and Lixin Ran

***Abstract*— Noncontact measurements of material parameters have important applications in various fields. In this paper, we propose a noncontact measurement of complex permittivity for electrically small samples at microwave frequencies. Based on Rayleigh approximation, we propose a noncontact measurement approach that can linearly retrieve complex permittivity from the measured impedance change. Using a subwavelength resonance, far-field radiation can be effectively suppressed, and thus the measurement is not notably influenced by unwanted environmental reflection. With the features of simple calibration and noncontact measurement, our method can be widely used in repeated on-site measurements of complex permittivity for small-sized samples at microwave frequencies.**

***Index Terms*— Complex permittivity, noncontact measurement, Rayleigh approximation, subwavelength resonance.**

## I. Introduction

COMPLEX permittivity is an important parameter describing the interaction between electromagnetic waves and materials. A convenient and accurate measurement of complex permittivity of materials is always desired in scientific research and industrial applications [1]–[3]. Until now, many effective methods have been invented to measure the complex permittivity for different frequency bands. At low frequencies, capacitance methods [4] and magnetic induction methods [5]–[7] are conventionally used. In the radio frequency (RF) and microwave bands, the transmission line methods [8]–[10], the resonance cavity methods [11], [12], and the free-space methods [13]–[15] are widely used.

Recently, noncontact and noninvasive measurement of complex permittivity has been attracting many interests [15]–[20]. Compared with contact measurements, such as the capacitance, transmission line, and resonance cavity methods, noncontact measurements, such as the magnetic induction and free space methods, do not require inserting special samples under test (SUTs) into measurement fixtures or waveguide cavities, and therefore have multiple advantages in the scenarios of on-site, desktop measurement of complex permittivity of a large number of SUTs.

For both the contact and noncontact measurements of complex permittivity, the key to obtain a high measurement precision is to utilize high quality factor ($Q$-factor) resonances [11], [14]. At low frequencies, the magnetic induction method based on high-$Q$-factor self-resonance coils is a good candidate for the noncontact measurement of complex permittivity. The difficulty of this method to achieve an optimal measurement precision is to match the impedance between the measurement instrument and the high-$Q$-factor resonant coil, which makes it difficult for the coil from obtaining the maximum resonance current. In our previous work [19], we introduced magnetically coupled, high-$Q$-factor resonant coils to the measurement setup of the conventional magnetic induction method to solve this difficulty. We also proposed an algorithm based on Rayleigh approximation to linearly retrieve the complex permittivity from the measured impedance data. However, high-$Q$-factor resonant coils can only be obtained at megahertz frequencies, and therefore, the magnetic induction method cannot be used in the noncontact measurement of complex permittivity in the RF and microwave bands.

At high frequencies, the free space methods originally developed for microwave remote sensing and imaging applications can be used for the noncontact measurement of complex permittivity [15]. However, this method is based on the inverse scattering problem instead of high-$Q$-factor resonances, and the measurement precision is thus not satisfactory. While using radiating far field, this method is not suitable for indoor use either, due to strong environmental reflections. If the

Manuscript received August 30, 2015; revised November 22, 2015, January 11, 2016, and June 27, 2016; accepted June 28, 2016. This work was supported by the NSFC under Grant 61131002, Grant 61528104, and Grant 61071063, by the ZJNSF under Grant LY16F010009, by the National Key Laboratory Foundation of China under Grant 9140C530203140C53232 and Grant 9140A20090314HT05310, by the Open Research Fund Program of the Key Laboratory for Spacecraft TT&C and Communication under Grant CTTC-FX201306, and by the Program for the Top Young Innovative Talents under Grant Q1313-03.

J. Dong is with the Laboratory of Applied Research on Electromagnetics, Zhejiang University, Hangzhou 310027, China, and also with the Science and Technology on Electromagnetic Compatibility Laboratory, China Ship Development and Design Center, Wuhan 430064, China (e-mail: dj19900805@zju.edu.cn).

F. Shen is with the China Research Institute of Radiowave Propagation, Xinxiang 453003, China (e-mail: sfz@zju.edu.cn).

Y. Dong, Y. Wang, and W. Fu are with the National Key Laboratory of Science and Technology on Space Microwave, Xi'an 710100, China (e-mail: yazhoudong@gmail.com; wangying_c504@163.com; wlfu-193@163.com).

H. Li, D. Ye, B. Zhang, J. Huangfu, and L. Ran are with the Laboratory of Applied Research on Electromagnetics, Zhejiang University, Hangzhou 310027, China (e-mail: xdlee07@163.com; desy@zju.edu.cn; aem@zju.edu.cn; huangfujt@zju.edu.cn; ranlx@zju.edu.cn).

S. Qiao is with the Department of Electronic Engineering, Zhejiang University City College, Hangzhou 310015, China (e-mail: qiaos@zucc.edu.cn).

Y. Sun is with the Nanjing Institute of Electronic Equipment, Nanjing 210007, China (yzsun8511@126.com).

C. Li is with the Department of Electrical and Computer Engineering, Texas Tech University, Lubbock, TX 79409 USA (e-mail: changzhi.li@ttu.edu).

Color versions of one or more of the figures in this paper are available online at http://ieeexplore.ieee.org.

Digital Object Identifier 10.1109/TMTT.2016.2588487

0018-9480 © 2016 IEEE. Personal use is permitted, but republication/redistribution requires IEEE permission.
See http://www.ieee.org/publications_standards/publications/rights/index.html for more information.

This article has been accepted for inclusion in a future issue of this journal. Content is final as presented, with the exception of pagination.



reflection/transmission measurement is used, this method also requires electrically large samples. In [20], a method based on near-field measurement was proposed based on a liftoff open-ended coaxial probe for large-sized samples along the radial direction. To the best of our knowledge, so far, there is no effective method that can be used in the precision noncontact measurement of complex permittivity of electrically small samples at the microwave and even higher frequencies with a linear retrieval equation.

In this paper, we extend our previously used approach to improve the conventional magnetic induction method and to obtain a new measurement setup that works at high frequencies in a wide range from RFs to millimeter wave frequencies [19], [21]. In order to facilitate desktop noncontact measurements and prevent unwanted environmental reflections from far-field radiation due to high-frequency resonances, we replace the magnetically coupled resonant coils with electrically coupled, high-$Q$-factor subwavelength split-ring resonators (SRRs) to effectively suppress the far-field radiation. In the meantime, the Rayleigh approximation-based algorithm is also derived for the new setup, providing a linear retrieval equation for the measured scattering parameters. Simulation and experimental results verify the effectiveness of the proposed approach. Based on the high-$Q$-factor subwavelength resonance and Rayleigh approximation, our method is able to wirelessly measure electrically small samples in open spaces, making it suitable for repeated desktop measurements of complex permittivity.

This paper is organized as follows. In Section II, the contact measurements based on SRRs and complementary SRRs (CSRRs) are introduced, and the working principle and the measurement algorithm of the proposed setup are derived. In Sections III and IV, simulations and experiments are presented, respectively, to verify the effectiveness of the proposed approach. Finally, a conclusion is drawn in Section V.

## II. Method and Algorithm

With deep subwavelength dimensions, SRRs and CSRRs have higher $Q$ factors than regular half-wavelength microstrip resonators. This property has been used in the contact measurement of dielectric contacts in the past years [22]–[24]. In order to compare the difference between our method and the existing SRR- and CSRR-based contact measurement methods, we will introduce the principle of both the methods in this section.

### A. Contact Methods

Fig. 1 shows a typical CSRR-based setup for contact measurement of complex permittivity, in which a CSRR etched on a metallic ground plane is fed by a microstrip line, and the SUTs are directly placed on the CSRR. In the contact measurement based on CSRRs and SRRs, the samples with a specified thickness should be large enough to completely cover the SRR or CSRR, so that relatively large frequency offsets due to these SUTs can be detected to retrieve the dielectric constants. Since SRRs or CSRRs fed by microstrip line normally have complicated equivalent circuits, analytical

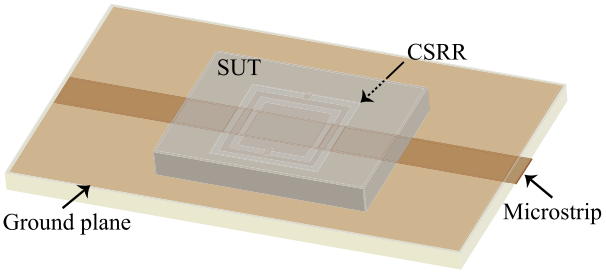


Fig. 1. Typical setup of CSRR-based contact measurement of complex permittivity.

retrieval equations are difficult to derive. In [22], the retrieval equation is assumed to be

$$\Delta f = A(\varepsilon_r)^2 + B\varepsilon_r + C \tag{1}$$

where $\varepsilon_r$ is the relative permittivity, $\Delta f$ is the frequency offset caused by the SUT, and $A$, $B$, and $C$ are the constants that can be calibrated by multiple known SUTs. For simplicity, in most works [24], the SUT is simply assumed to linearly affect the total capacitance and/or inductance of the SRR or CSRR. In this case, the dielectric constant can be calculated as

$$\varepsilon_r = A_1(\Delta f)^{-2} \tag{2}$$

and the calibration of constant $A_1$ only needs one known SUT.

For the contact measurements based on SRRs and CSRRs, the advantage is the high sensitivity due to the high-$Q$ factor of subwavelength resonance, and the disadvantage is the large impact to the measurement results due to the existence of thin air gaps between the SUTs and the SRRs/CSRRs. The latter issue significantly affects the precision and stability of such contact measurements, requiring the surfaces of both the SRR/CSRR and the SUT to be highly flat.

### B. Noncontact Method

As mentioned, a natural extension of the approach proposed in [19] is to replace the resonant coils with high-$Q$-factor, subwavelength SRR to achieve measurement frequencies from RF to millimetre-wave bands, as shown in Fig. 2(a). In order to obtain a strongly coupled subwavelength resonance, a standard microstrip line with characteristic impedance $Z_c$ is used to excite the resonance of the SRR. Different from conventional SRRs used in metamaterials [25], [26], such an SRR is also backed with a ground plane. By doing so, the dimension of the SRR can be reduced to one tenth of the wavelength to further increase the resonant $Q$ factor and suppress the far-field radiation.

With noncontact measurements, SUTs are no longer placed on the SRR, and therefore, the issue due to an air gap can be effectively avoided. For a deep subwavelength SRR, its far-field range is very small, and therefore, SUTs can still be placed close to the SRR for their impacts to the subwavelength resonance to be easily sensed within the dynamic range of the measurement instrument. Another major difference between the contact and noncontact measurements is that noncontact measurements are based on the change of the impedance

This article has been accepted for inclusion in a future issue of this journal. Content is final as presented, with the exception of pagination.



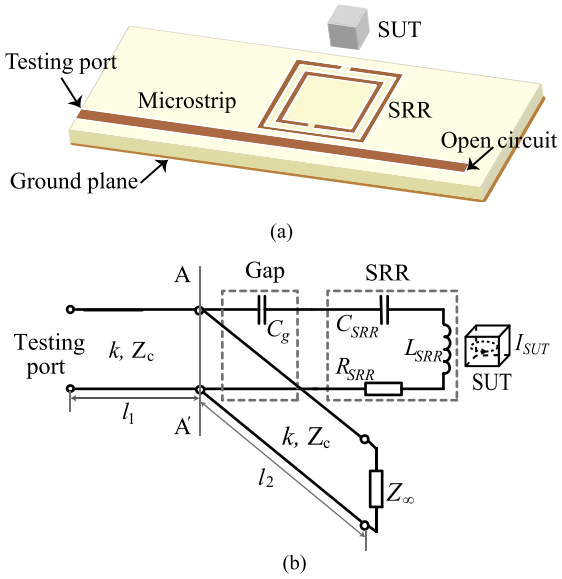


Fig. 2. Noncontact measurement setup based on gap-coupled subwavelength SRR. (a) Schematic. The SUT is placed over the SRR with an air gap in-between. (b) Equivalent circuit model.

(or equivalently the reflection coefficient), whereas contact measurements are based on the change of resonant frequency. Therefore, the retrieval algorithm used in the noncontact measurement will be completely different. Without notable frequency offsets, this also allows to measure the complex permittivity of different SUTs at the same frequency.

In Fig. 2(b), we present the equivalent circuit model of Fig. 2(a), where the SRR is electrically excited through a gap capacitance $C_g$ [27], and the SRR is equivalent to a series *RLC* resonant network. Note that $C_g$ depends on the width and length of the gap between the microstrip and the SRR. Based on Fig. 2(b), the impedance of the microstrip line in the absence of the SUT at location $AA'$ is

$$Z_{AA'} = \frac{1}{1/(1/j\omega C_g + Z_{\mathrm{SRR}}) + 1/X_L} \tag{3}$$

where $Z_{\mathrm{SRR}} = R_{\mathrm{SRR}} + j\omega L_{\mathrm{SRR}} + 1/j\omega C_{\mathrm{SRR}}$ is the equivalent impedance of the SRR seen from the microstrip line and $X_L$ is a constant reactance due to the open-circuit load and the length $l_2$ of the microstrip line. The impedance matching at location $AA'$ requires $Z_{AA'} = Z_c$ at the resonant frequency. According to transmission line theory, this can always be obtained by tuning $l_2$ and the gap capacitance $C_g$. Note that $X_L$ changes in a wide range when tuning $l_2$, and tuning $C_g$ can effectively impact the resistance of $Z_{AA'}$ [19].

Furthermore, the impedance of the microstrip line in the presence of the SUT at location $AA'$ is

$$Z'_{AA'} = \frac{1}{1/(1/j\omega C_g + Z_{\mathrm{SRR}} + \Delta Z_{\mathrm{SRR}}(\tilde{\varepsilon}_r, \omega)) + 1/X_L} \tag{4}$$

where $\Delta Z_{\mathrm{SRR}}(\tilde{\varepsilon}_r, \omega)\Delta Z_{\mathrm{SRR}}(\tilde{\varepsilon}_r, \omega)$ is the perturbation of $Z_{\mathrm{SRR}}$ due to the SUT and $\tilde{\varepsilon}_r$ is the complex permittivity of the SUT. Accordingly, the change of the reflection coefficient ($S_{11}$) due to the SUT can be derived as

$$\Delta S_{11} = \left(\frac{Z'_{AA'} - Z_c}{Z'_{AA'} + Z_c} - \frac{Z_{AA'} - Z_c}{Z_{AA'} + Z_c}\right) e^{-j2kl_1} \tag{5}$$

where $l_1$ is the distance between $AA'$ and the testing port, and $k$ is the wave number of the microstrip line.

According to [28]

$$\Delta Z_{\mathrm{SRR}} = \frac{j\omega\varepsilon_0}{I^2} \iiint \bar{E}_{\mathrm{inc}}(\bar{r}) \cdot [(\tilde{\varepsilon} - 1) \cdot \bar{E}_{\mathrm{tot}}(\bar{r})] dV \tag{6}$$

where $I$ is the resonant current and/or displacement current flowing in the SRR, and $\bar{E}_{\mathrm{inc}}$ and $\bar{E}_{\mathrm{tot}}$ are the incident and total fields, respectively. When the size of the SUT is sufficiently smaller than the wavelength, Rayleigh approximation can be used to calculate $\bar{E}_{\mathrm{tot}}$ [29]. In this case, the backscattered field sensed by the SRR can be expressed as

$$E_{\mathrm{sca}} = -\left(\frac{\tilde{\varepsilon}_r - 1}{\tilde{\varepsilon}_r + 2}\right) \varepsilon_0 k_0^2 \frac{a^3}{R^2} E_0 e^{ik_0 r} \tag{7}$$

where $R$ is the distance between the SRR and the SUT, $a^3$ is the volume of the SUT, $k_0$ is the wave vector in the air, and $E_0$ is the amplitude of the electric field transmitted by the SRR [29]. Then, the total field in the position of the SRR is

$$E_{\mathrm{tot}} = \frac{3}{\tilde{\varepsilon}_r + 2} \varepsilon_0 k_0^2 \frac{a^3}{R^2} E_0 e^{ik_0 r}. \tag{8}$$

Substituting (8) into (6), we have

$$\Delta Z_{\mathrm{SRR,Rayleigh}} = \kappa_1 \cdot \frac{\tilde{\varepsilon}_r - 1}{\tilde{\varepsilon}_r + 2} \tag{9}$$

where $\kappa_1$ is a complex constant proportional to $a^3/R^2$.

Under the Rayleigh assumption, we can also derive

$$\Delta S_{11} = \kappa_2 \cdot \Delta Z_{\mathrm{SRR,Rayleigh}} \tag{10}$$

where $\kappa_2$ is a constant determined by the setup (See the Appendix). Substituting (9) into (10), we obtain

$$\Delta S_{11} = \alpha \frac{\tilde{\varepsilon}_r - 1}{\tilde{\varepsilon}_r + 2} \tag{11}$$

where $\alpha = \kappa_1\kappa_2$. Similar to $\kappa_1$, for a given setup, $\alpha$ is a complex constant proportional to $a^3/R^2$. It is seen that once $\alpha$ is determined, $\tilde{\varepsilon}_r$ can be directly obtained from (11). If $\Delta S_{11}$ for a reference SUT with a known $\tilde{\varepsilon}_r$ is measured, $\alpha$ for this setup can be obtained by (11).

It is worth noting that compared with our previous work aiming to improve the magnetic induction method, which is used the change of impedance for the retrieval algorithm, this paper uses the change of $S_{11}$. The reason is that the distance between $AA'$ and the testing port can hardly be accurately obtained. An additional advantage of using the change of $S_{11}$ is that the calibration of the measurement setup only needs two simple steps, instead of three steps in the previous method, as will be illustrated in the following.

This article has been accepted for inclusion in a future issue of this journal. Content is final as presented, with the exception of pagination.



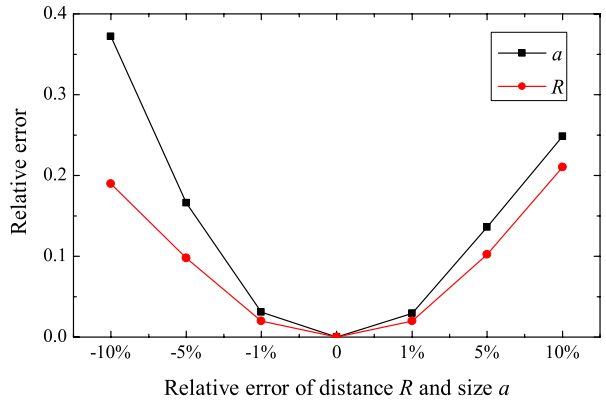


Fig. 3. Error analysis for the inaccuracy of the position and the size of SUTs.

### C. Errors and Measurement Uncertainty

Since the complex permittivity has a nonlinear relationship with $R$ and $a$, it is difficult to directly calculate the relative error of the measured complex permittivity due to the errors in the distance between the SRR and the SUT and the size of the SUT. According to (11)

$$\frac{\tilde{\varepsilon}_r - 1}{\tilde{\varepsilon}_r + 2} \infty \Delta S_{11} R^2 / a^3. \tag{12}$$

Therefore, we can first calculate the relative error of $(\tilde{\varepsilon}_r - 1)/(\tilde{\varepsilon}_r + 2)$, which is defined as

$$\delta = \frac{|(\Delta S_{11} R^2/a^3)_{\text{error}} - (\Delta S_{11} R^2/a^3)_{\text{true}}|}{|(\Delta S_{11} R^2/a^3)_{\text{true}}|} \tag{13}$$

and then further evaluate the error of the measured complex permittivity using a simple calculation. Fig. 3 shows the errors calculated by (13) with respect to the relative errors of $R$ and $a$. To be consistent with the following simulation and experiment, we assume the true values of $R$ and $a$ as 7 and 10 mm, respectively. It is seen that when the relative error of $a$ or $R$ is larger than 5%, the error of $(\tilde{\varepsilon}_r - 1)/(\tilde{\varepsilon}_r + 2)$ begins to exceed 10%, and the changing rate of such an error is much faster for lager errors of $a$ or $R$.

According to (7), the scattered field is inversely proportional to $R^2$. This is the reason why a small error of $R$ could potentially result in a notable error of the retrieved result. However, when the far-field range condition is satisfied, a small position error in the horizontal direction would not lead to a notable change in $R$. In this case, the retrieved result would not be sensitive to the small position error in the horizontal direction.

According to (12) and [30], we can also derive the type B measurement uncertainty of $(\tilde{\varepsilon}_r - 1)/(\tilde{\varepsilon}_r + 2)$ as

$$\begin{aligned} U_{\varepsilon B} &= \sqrt{(\partial f/\partial \Delta S_{11})^2 U_{\Delta S_{11}}^2 + (\partial f/\partial R)^2 U_R^2 + (\partial f/\partial a)^2 U_a^2} \\ &= R/(\xi a^3) \cdot \sqrt{R^2 U_{\Delta S_{11}}^2 + 4\Delta S_{11}^2 U_R^2 + (9\Delta S_{11}^2 R^2/a^2) U_a^2} \end{aligned} \tag{14}$$

where $\xi = \alpha R^2/a^3$, $U_{\Delta S11}$, $U_R$, and $U_a$ are the uncertainty values of $\Delta S_{11}$, distance $R$, and volume $a^3$, respectively. Therefore, once $U_{\Delta S11}$, $U_R$, and $U_a$ are evaluated, the measurement uncertainty of the proposed method can be obtained as well.

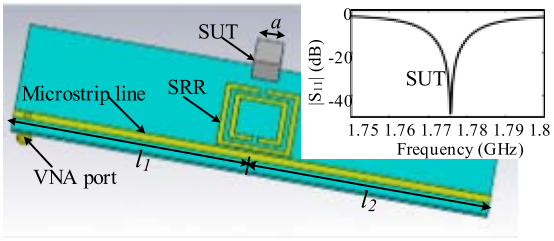


Fig. 4. Simulation setup for the calibration of (12).

## III. Simulation

### A. Simulation Setup and Its Calibration

In order to verify the retrieval algorithm derived in Section II, full-wave simulations are first performed using a commercial Maxwell Equations solver, CST microwave studio. The simulation model is shown in Fig. 4, which is in accordance with Fig. 2(a). In the simulation model, a conventional square SRR with the side length of 14 mm is printed on a 0.762-mm-thick Rogers 4350B substrate with a dielectric constant of 3.48 and a loss tangent of 0.0037. The width of the copper strips of the SRR and the spacing between these strips are both 1.0 mm. The SRR is coupled to a 1.74-mm-wide 50-Ω microstrip line through a 0.4-mm gap. The lengths $l_2$ and $l_1$ shown in Fig. 2(a) are both 60 mm. A 50-Ω coaxial waveguide port is configured as a VNA port. The simulated reflection coefficient without an existence of SUT is shown in Fig. 4 (inset). It is seen that $S_{11}$ is lower than −40 dB at 1.776 GHz, implying a very high-$Q$-factor resonance of the SRR. At this frequency, the SRR is only 8.3% of the corresponding wavelength, having very low far-field radiation efficiency.

In the simulation with SUTs, we first simulate a lossless SUT, whose dielectric constant is scanned from 1 to 20. In order to investigate if the condition of the Rayleigh approximation is satisfied, the side length of the cubic SUT is also scanned from 6 to 12 mm, corresponding to 3.6%–7.1% of the wavelength. In the simulation, the SUT is placed 7 mm away from the SRR. Note that at 1.776 GHz, the far-field range of the SRR is 4.6 mm if calculated by its diagonal line. The amplitude and phase of simulated $S_{11}$ data for the SUT with side length $a = 10$ mm are shown in Fig. 5.

It is seen that with an increased dielectric constant, the resonant frequency of the SRR slightly changes to the lower frequency in a negligible range; however, the maximum change of the amplitude and phase of $S_{11}$ data in the vicinity of the original resonant frequency are 5.2 dB and 53°, respectively, which are notably large for the retrieval of complex permittivity from these data.

In order to calibrate the simulation setup, we choose the SUT whose dielectric constant is 2.0 as the reference, to obtain $\alpha$ by (11). For the simulation setup shown in Fig. 4, $\alpha$ is calculated as 0.0033 – j0.0083. It is seen that the calibration of the measurement setup is very convenient. However, if the size and location of SUTs are changed, the measurement setup should be recalibrated using the new reference SUT.

This article has been accepted for inclusion in a future issue of this journal. Content is final as presented, with the exception of pagination.



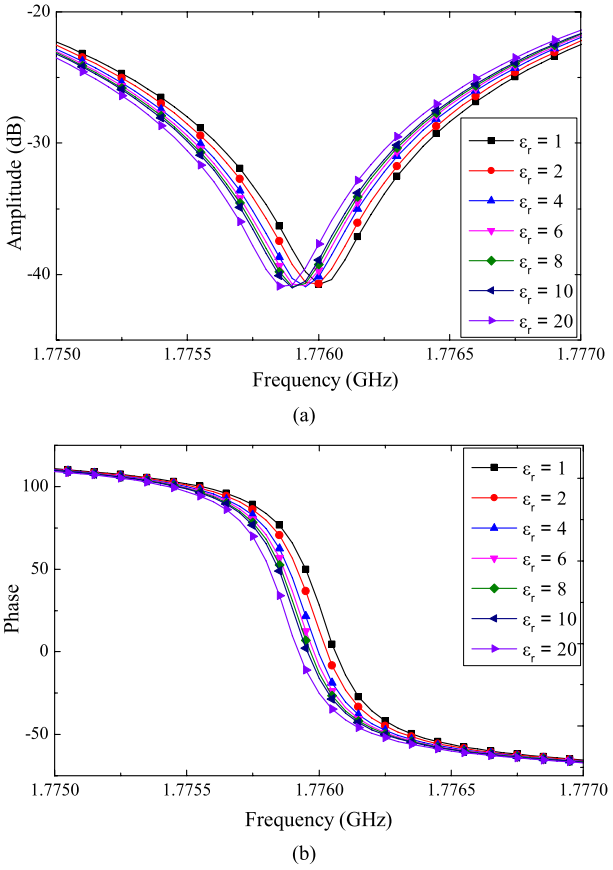


Fig. 5. Simulation results of $S_{11}$ curves for SUTs with different dielectric constants from 1 to 20. (a) Amplitudes. (b) Phases.

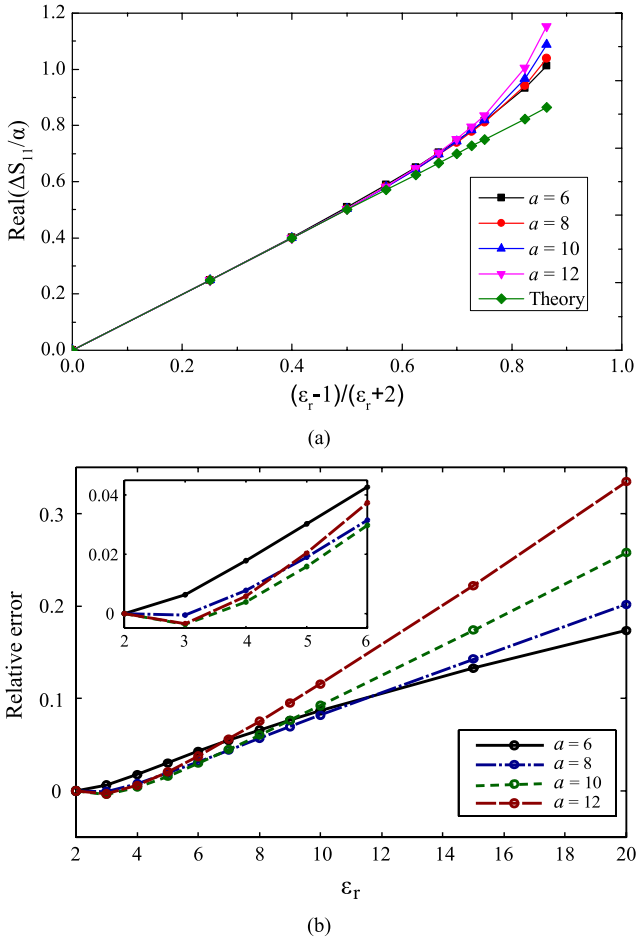


Fig. 6. (a) Comparison between theoretical and simulated results for SUTs with different sizes. (b) Error analysis.

### *B. Retrieval Results From Simulation Data*

After the simple calibration, (11) can be used to calculate both the real and imaginary parts of the complex permittivity of different SUTs from the measured $S_{11}$ data. Fig. 6(a) shows the simulated $\Delta S_{11}/\alpha$ with respect to $(\varepsilon_r - 1)/(\varepsilon_r + 2)$ at the resonance frequency of 1.776 GHz for SUTs with $a = 6$, 8, 10, and 12 mm, as compared with the theoretical value based on (11). It is seen that the simulated result complies well with the theoretical curve when $(\varepsilon_r - 1)/(\varepsilon_r + 2)$ is smaller than 0.5. When $(\varepsilon_r - 1)/(\varepsilon_r + 2)$ is larger than 0.5, corresponding to $\varepsilon_r$ being larger than 4, the theoretical curves begin to deviate from the simulated curve, implying that the measurement error based on the assumption of Rayleigh approximation would increase.

In Fig. 6(b), the errors of the retrieved dielectric constants with respect to the simulated result are shown. The error is defined as (13), which reflects the error between the simulated perturbation of the scattering due to the SUT and the perturbation calculated by Rayleigh approximation. It is seen that for dielectric constants larger than 9, the error begins to exceed 10%, and the increase of the measurement error is much faster for SUTs with higher dielectric constants. However, if a 5% or lower error is required, the measured dielectric constant should be lower than 5.

Based on Fig. 6(b), the error becomes larger with the increase of the dimension and the dielectric constant. Therefore, the required size of the SUT would depend on the needed accuracy. For example, in order to obtain a less than 10% error, the dimension of the SUT should be smaller than 6% of the wavelength for dielectric constants less than 10. On the other hand, we see from Fig. 6(b) that, as long as the electrical size of SUTs satisfies the Rayleigh approximation, the relative errors between those of different SUTs are small. This result indicates that if it is desired to measure the dielectric constants in a wide range, only a few number of standard size of SUTs are needed.

Fig. 7 shows the retrieved permittivity of three SUTs from the simulated $S_{11}$ data in the frequency range between 1.75 and 1.8 GHz, when the dielectric constants of SUTs are 3, 4, and 5, respectively. Both the real and imaginary parts form parallel lines in the resonance region, which can be easily discriminated. The retrieval results show that all the imaginary parts of permittivity are close to zero, which is consistent with the expectation. The calculated real parts are 2.99, 4.02, and 5.15, and the relative errors are 0.3%, 0.5%, and 3%, respectively. The trend of the increased error also complies with the above analysis. Since the condition to satisfy the Rayleigh approximation fully depends on the electric size of the SUT, a better result can always be obtained by decreasing the size of an SUT whose permittivity is relatively large.

This article has been accepted for inclusion in a future issue of this journal. Content is final as presented, with the exception of pagination.



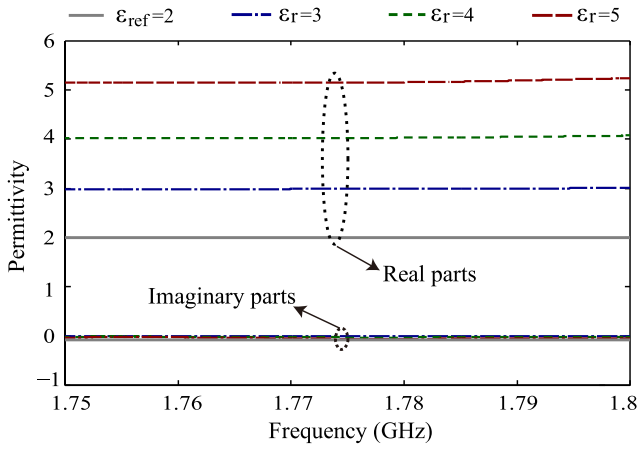


Fig. 7. Retrieved complex permittivity for SUTs with dielectric constants of 3, 4, and 5.

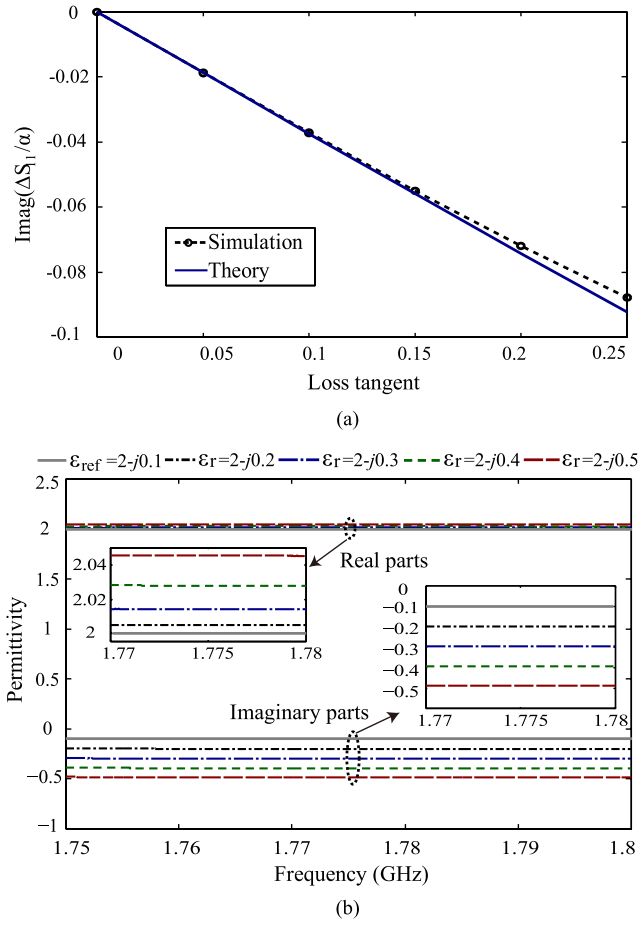


Fig. 8. (a) Comparison between theoretical and simulation results for lossy SUTs. (b) Retrieved results.

Similarly, we can also investigate the retrieval of permittivity when SUT samples are lossy. Fig. 8(a) shows the simulated and theoretical results for the same SUT with a dielectric constant of 2.0 and loss tangent varying from 0 to 0.25. It is seen that the simulation results comply with the Rayleigh approximation until the loss tangent is larger than 0.15. This implies that the proposed method can be used in the measurement of lossy media.

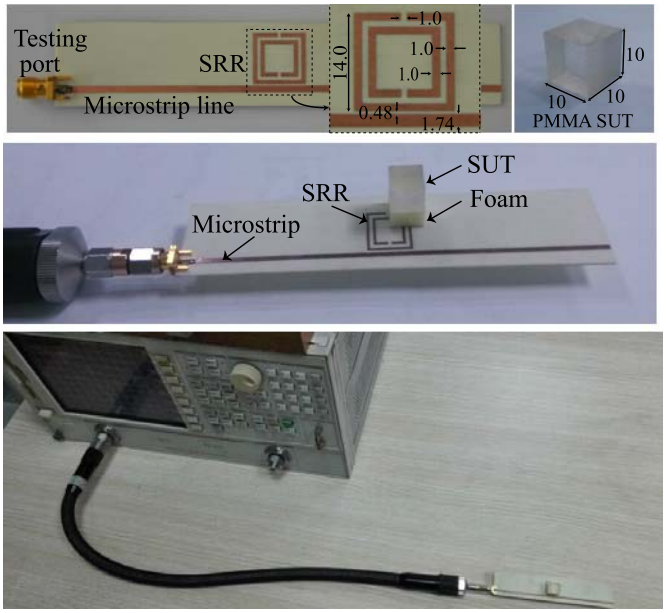


Fig. 9. Experimental setup.

Furthermore, we simulated four SUTs whose complex permittivities are 2 − j0.1, 2 − j0.2, 2 − j0.3, 2 − j0.4, and 2 − j0.5, respectively. Fig. 8(b) shows the permittivity of four SUTs retrieved from the simulated $S_{11}$ data with $\alpha$ calibrated by the SUT with a permittivity of 2 – j0.1. It is seen that both the real and imaginary parts form parallel lines in the resonance region. All the retrieved real parts are very close to 2, and the corresponding imaginary parts are –j0.199, –j0.297, –j0.393, and –j0.486, respectively, and are also consistent with the known conditions. Note that a loss tangent of 0.25 corresponds to a quite lossy medium.

## IV. Experimental Measurement

In order to validate the derived retrieval algorithm and the simulation results, an experimental setup that is the same as the simulation model was fabricated, as shown in Fig. 9. An Agilent 8722ES VNA is used to measure the change in $S_{11}$. Its frequency resolution and noise floor are 1 Hz and −118 dBm, respectively. Before measurement, it was calibrated with the standard short, open, load, thru method. In the measurement, the power level and the intermediate frequency bandwidth were set as −15 dBm and 10 Hz, respectively. The measurement using the fabricated setup without any SUT shows that the resonance frequency of the SRR is 1.8023 GHz, slightly different from the simulation case.

In the measurement, it is important to ensure the validation of Rayleigh approximation, which assumes a plane-wave excitation. In practice, whether the phase front of an incident wave is sufficiently flat is determined by the distance between the source and the object. When such a distance is larger than the radiation far-field range, which is normally calculated by $2(D^2 + d^2)/\lambda$, where $D$ and $d$ represent the size of the source and SUT, respectively, the plane-wave assumption can be considered to be valid [27].

This article has been accepted for inclusion in a future issue of this journal. Content is final as presented, with the exception of pagination.



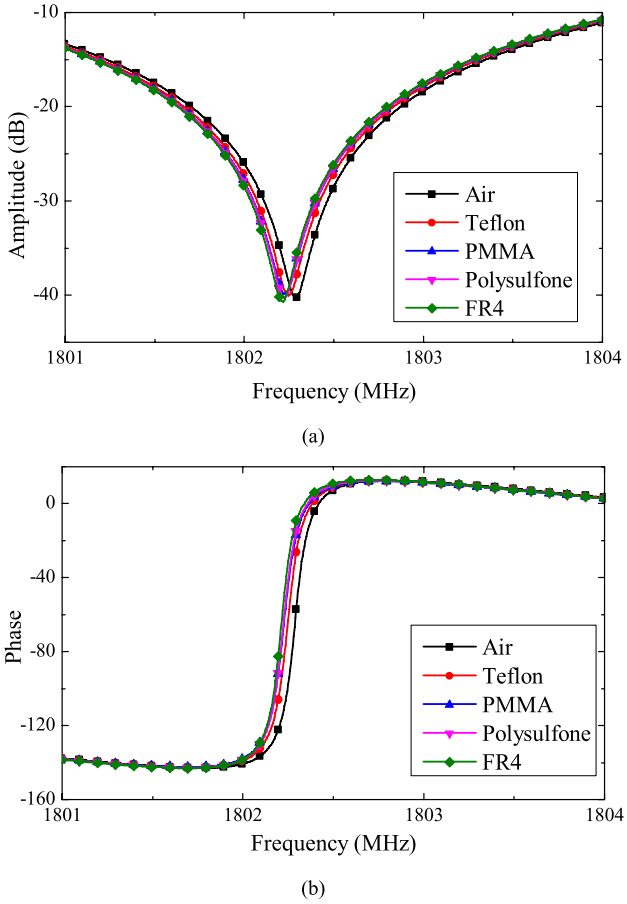


Fig. 10. Measured results of $S_{11}$ curves for air, Teflon, PMMA, polysulfone, and FR4 materials. (a) Amplitudes. (b) Phases.

In the measurements, we used the 10-mm cubic SUTs. For the 1.8 GHz resonant frequency, the size of SUT is around 6% of the wavelength. In the measurements, four SUTs made of Teflon, polymethyl methacrylate (PMMA), polysulfone, and FR4 materials, respectively, were measured, and the Teflon SUT is used as the reference. In all the measurements, the SUTs were placed 7 mm from the SRR with a 7-mm-thick foam spacing. Since the size of the SRR is 1.4 cm, the corresponding far-field range is 3.5 mm, which is much shorter than the 7 mm spacing. This location can be arbitrarily chosen, as long as the SUTs are placed at the same location as that of the reference SUT, and the measured impedance change has a good signal-to-noise ratio. A photograph of the fabricated experimental setup and the PMMA SUT are shown in Fig. 9.

Fig. 10 shows the measured amplitude and phase of the $S_{11}$ data for the setup with and without various types of SUTs. It is seen that the experimental results are consistent with the simulation results. At the resonance frequency of 1.8023 GHz, the changes of the amplitude and phase of the measured $S_{11}$ data are 5.7 dB and 45 degrees, respectively. To calibrate the experimental setup, we choose the Teflon sample with a known complex permittivity of $2.1 - j0.004$ as the reference. The calculated real and imaginary parts of $\alpha$ are shown in Fig. 11.

Fig. 12(a) shows the measured $S_{11}$ change ($\Delta S_{11}/\alpha$) in a bandwidth of 3 MHz between 1.801 and 1.804 GHz

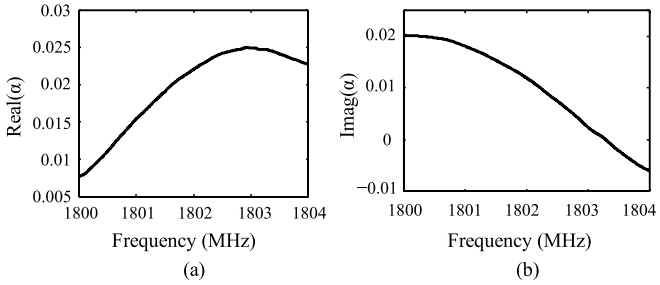


Fig. 11. (a) Real and (b) imaginary parts of the factor $\alpha$.

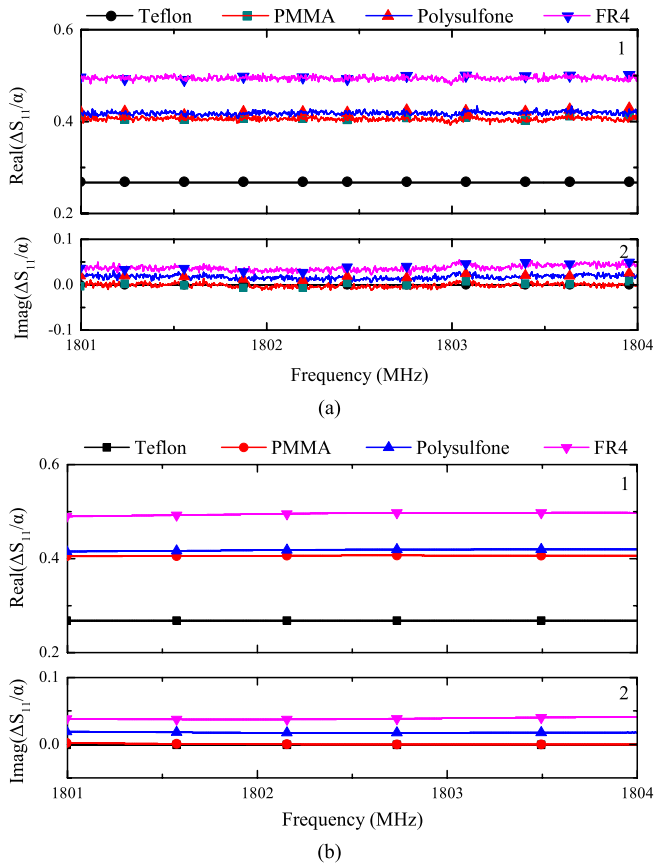


Fig. 12. Measured results for Teflon, PMMA, polysulfone, and FR4 SUTs. (a) Raw data. (b) Filtered data.

without any filtering. Such a narrow bandwidth ensures that the minimum resolution bandwidth of the VNA can be used to achieve the best noise performance. However, we can still see the random noise caused by the limited resolution of the VNA, i.e., 0.01 dB. In comparison, an average filter was applied to transform Fig. 12(a) to (b) [31]. Fig. 12(b) shows the filtered $S_{11}$ change ($\Delta S_{11}/\alpha$) in the same band. In this case, both the real and imaginary parts of $\Delta S_{11}/\alpha$ are measured for Teflon, PMMA, polysulfone, and FR4 SUTs. The smooth, quasi-parallel lines imply a high measurement resolution due to the high-$Q$-factor resonance, especially in the grayed zones between 1.8019 and 1.8028 GHz.

Based on (11) and the calibrated curves of $\alpha$, we can obtain the measured complex permittivities for PMMA, polysulfone, and FR4 SUTs as $3.05 - j0.05$, $3.15 - j0.15$, and $3.95 - j0.4$, respectively. The corresponding loss tangents

This article has been accepted for inclusion in a future issue of this journal. Content is final as presented, with the exception of pagination.



TABLE I
COMPARISON BETWEEN THE EXPERIMENTAL RESULTS MEASURED WITH DIFFERENT METHODS

| | Teflon | PMMA | Polysulfone | FR4 |
|---|---|---|---|---|
| Nominal ranges | 2.0~2.1 | 3.0-3.6 | ~3.06 | 4.0-4.6 |
| Waveguide method | 1.96 | 2.74 | 2.98 | 4.07 |
| This work | 2.1 | 3.05 | 3.15 | 3.95 |
| Error | 7.1% | 11.3% | 5.7% | 2.9% |

are 0.016, 0.048, and 0.10. Table I presents the comparison between the measured dielectric constant of the SUTs with respect to their nominal ranges [32]–[34]. In addition, we also established an $L$-band measurement system based on the standard waveguide method [35]. In this system, a WR430 rectangular waveguide and an Agilent 8722ES network analyzer were used, and the samples were processed into thin rectangular slabs with the same cross section as the waveguide. The retrieved results are also listed in Table I. It is seen that all the measured results are close to the nominal values and the experimental results obtained by the waveguide method within reasonable floating ranges.

Although the measured real parts of the SUTs' permittivity are satisfactory, we can notice that the measurement errors of imaginary parts are relatively large. For the FR4 SUT whose loss tangent is normally 0.02, the measured result is 0.10. This error comes from the resolution limitation of the VNA. In Fig. 12(a), we can see that for both real and imaginary parts, the amplitudes of the noise are on the same level. However, the values of the real parts are one order higher than those of the imaginary parts. This will absolutely introduce a larger measurement error to the imaginary parts.

To clarify this issue, we can introduce small noises to the simulated $S_{11}$ data for SUTs with different imaginary parts. Fig. 13(a) and (b) shows the retrieved real and imaginary parts of SUTs whose complex permittivities are set as $2 - j0.02$, $2 - j0.03$, $2 - j0.04$, and $2 - j0.05$, where 0.001 and 0.01 dB white noises are introduced to the simulated data, respectively. Compared with the ideal case without any noise, as shown in Fig. 8, the introduction of these noises results in notable noises in the retrieved results, especially in the nonresonant regions. For the 0.001-dB noise, the retrieved imaginary parts can still be separated. However, for the 0.01-dB noise, the retrieved imaginary parts overlap with each other. In the meantime, the measurement errors of real parts in both the cases are acceptable within the resonance range. This result complies with what we observed in Fig. 12(a), i.e., the low noise could seriously impact the measurement error of the imaginary part when an SUT has a small loss tangent. This also reminds us that when SUTs with very small losses are measured, a VNA with sufficiently high measurement resolution should be used.

In Fig. 13(c), the imaginary parts of the above SUTs are further increased to $-j0.2$, $-j0.3$, $-j0.4$, and $-j0.5$, respectively, and the introduced noise remains to be 0.01 dB. It is seen that

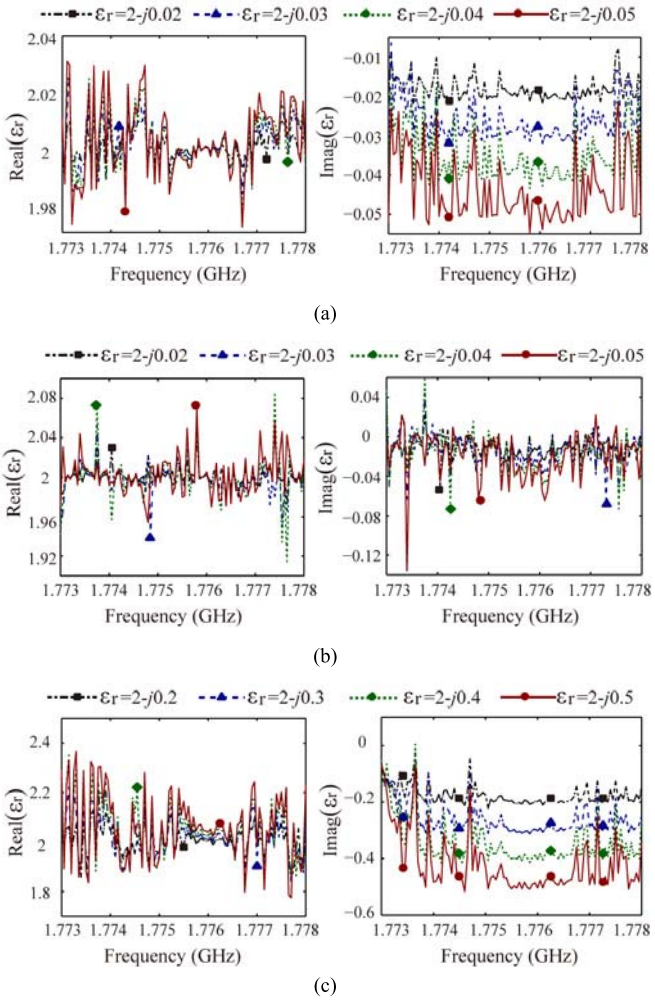


Fig. 13. Measurement error analysis when small noises are introduced to the simulated data for SUTs with different imaginary parts, where (a) 0.001, (b) 0.01, and (c) 0.01-dB white noises are introduced to the simulated data with different imaginary parts.

with the same noise, both the real and imaginary parts of the retrieved complex permittivities can be clearly discriminated again, implying that the proposed method can be widely used in measuring SUTs with large losses.

Apart from the Rayleigh approximation, the measurement results also include errors caused by other factors, such as the measured error of $\Delta S_{11}$, the fabrication precision of SUTs, and the position error between the reference SUT and other SUTs. With noncontact measurements, it avoids placing the SUTs in the immediate near-field range of the resonance SRR. However, these errors, especially the position error, can still significantly impact the stability of the final results. In practical applications, the measurement setup should be carefully designed and fabricated to avoid such influences.

## V. CONCLUSION

In conclusion, the measurement setup, retrieval algorithm, simulation and experimental verification of the noncontact measurement of complex permittivity for electrically small SUTs based on coupled subwavelength resonance, and Rayleigh approximation are introduced. The low-cost, desktop

This article has been accepted for inclusion in a future issue of this journal. Content is final as presented, with the exception of pagination.



measurement setup can be easily fabricated and calibrated, and the measurement frequency can be extended to higher microwave- and millimeter-wave frequencies. Being able to wirelessly measure the complex permittivity, we expect our method can be widely used in the repeated on-site measurements of complex permittivity of various materials.

## APPENDIX

According to (5)

$$\Delta S_{11} = \left(\frac{Z'_{AA'} - Z_c}{Z'_{AA'} + Z_c} - \frac{Z_{AA'} - Z_c}{Z_{AA'} + Z_c}\right) e^{-j2kl_1} = \frac{2Z_c(Z'_{AA'} - Z_{AA'})}{(Z'_{AA'} + Z_c)(Z_{AA'} + Z_c)} e^{-j2kl_1} \tag{A1}$$

Denote $Z_0 = 1/j\omega C_g + Z_{\mathrm{SRR}}$

$$Z'_{AA'} - Z_{AA'} = \frac{1}{\frac{1}{1/j\omega C_g + Z_{\mathrm{SRR}} + \Delta Z_{\mathrm{SRR}}} + \frac{1}{X_L}} - \frac{1}{\frac{1}{1/j\omega C_g + Z_{\mathrm{SRR}}} + \frac{1}{X_L}} = \frac{\Delta Z_{\mathrm{SRR}} X_L}{(Z_0 + \Delta Z_{\mathrm{SRR}} + X_L)(Z_0 + X_L)}. \tag{A2}$$

Substituting (A2) into (A1), we have

$$\Delta S_{11} = \frac{2Z_c \Delta Z_{\mathrm{SRR}} X_L}{(Z'_{AA'} + Z_c)(Z_{AA'} + Z_c)(Z_0 + \Delta Z_{\mathrm{SRR}}) Z_0} e^{-j2kl_1}. \tag{A3}$$

Under the Rayleigh approximation, the reflection due to the SUT is very weak. Therefore, the perturbation item $\Delta Z_{\mathrm{SRR}}$ is also very small. In this case, the item $\Delta Z_{\mathrm{SRR}}$ in the denominator of $\Delta S_{11}$ can be neglected, and (A3) can be written as

$$\Delta S_{11} = \kappa_2 \cdot \Delta Z_{\mathrm{SRR,Rayleigh}} \tag{A4}$$

where $\kappa_2$ is a constant determined by the impedance and length of transmission lines used in the measurement setup.

## REFERENCES


[1] U. Kaatze and Y. Feldman, "Broadband dielectric spectrometry of liquids and biosystems," *Meas. Sci. Technol.*, vol. 17, no. 2, pp. R17–R35, Feb. 2006.

[2] S. O. Nelson and S. Trabelsi, "Dielectric spectroscopy measurements on fruit, meat, and grain," *Trans. Amer. Soc. Agricult. Biol. Eng.*, vol. 51, no. 5, pp. 1829–1834, Sep. 2008.

[3] U. Kaatze, "Techniques for measuring the microwave dielectric properties of materials," *Metrologia*, vol. 47, no. 2, pp. S91–S113, Mar. 2010.

[4] W. J. K. Raymond, C. K. Chakrabarty, G. C. Hock, and A. B. Ghani, "Complex permittivity measurement using capacitance method from 300 kHz to 50 MHz," *Measurement*, vol. 46, no. 10, pp. 3796–3801, Dec. 2013.

[5] H.-Y. Wei and M. Soleimani, "Electromagnetic tomography for medical and industrial applications: Challenges and opportunities [point of view]," *Proc. IEEE*, vol. 101, no. 3, pp. 559–565, Mar. 2013.

[6] H. Griffiths, "Magnetic induction tomography," *Meas. Sci. Technol.*, vol. 12, no. 8, pp. 1126–1131, Jun. 2001.

[7] I. Yu, "Electrodeless measurement of RF dielectric constant and loss," *Meas. Sci. Technol.*, vol. 4, pp. 344–348, Apr. 1993.

[8] J. Baker-Jarvis, M. D. Janezic, J. H. Grosvenor, Jr., and R. G. Geyer, "Transmission/reflection and short-circuit line methods for measuring permittivity and permeability," Nat. Inst. Standards Technol., Boulder, CO, USA, Tech. Note 1355-R, May 1992.

[9] D. V. Blackham and R. D. Pollard, "An improved technique for permittivity measurements using a coaxial probe," *IEEE Trans. Instrum. Meas.*, vol. 46, no. 5, pp. 1093–1099, Oct. 1997.

[10] M. N. M. Kehn, L. Shafai, F. Safari, and S. Noghanian, "Permittivity measurement of disk and annular dielectric samples using coaxial transmission line fixtures. Part II: Experimentation and accuracy analyses," *Can. J. Elect. Comput. Eng.*, vol. 34, nos. 1–2, pp. 31–41, 2009.

[11] S. Li, C. Akyel, and R. G. Bosisio, "Precise calculations and measurements on the complex dielectric constant of lossy materials using $TM_{010}$ cavity perturbation techniques," *IEEE Trans. Microw. Theory Techn.*, vol. MTT-29, no. 10, pp. 1041–1048, Oct. 1981.

[12] B. Meng, J. Booske, and R. Cooper, "Extended cavity perturbation technique to determine the complex permittivity of dielectric materials," *IEEE Trans. Microw. Theory Techn.*, vol. 43, no. 11, pp. 2633–2636, Nov. 1995.

[13] C. Yu *et al.*, "Active microwave imaging II: 3-D system prototype and image reconstruction from experimental data," *IEEE Trans. Microw. Theory Techn.*, vol. 56, no. 4, pp. 991–1000, Apr. 2008.

[14] C. Orlob, T. Reinecke, E. Denicke, B. Geck, and I. Rolfes, "Compact unfocused antenna setup for X-band free-space dielectric measurements based on line-network-network calibration method," *IEEE Trans. Instrum. Meas.*, vol. 62, no. 7, pp. 1982–1989, Jul. 2013.

[15] D. K. Ghodgaonkar, V. V. Varadan, and V. K. Varadan, "Free-space measurement of complex permittivity and complex permeability of magnetic materials at microwave frequencies," *IEEE Trans. Instrum. Meas.*, vol. 39, no. 2, pp. 387–394, Apr. 1990.

[16] A. Barai, S. Watson, H. Griffiths, and R. Patz, "Magnetic induction spectroscopy: Non-contact measurement of the electrical conductivity spectra of biological samples," *Meas. Sci. Technol.*, vol. 23, no. 8, p. 085501, Jun. 2012.

[17] H. Lobato-Morales, A. Corona-Chávez, J. L. Olvera-Cervantes, R. A. Chávez-Pérez, and J. L. Medina-Monroy, "Wireless sensing of complex dielectric permittivity of liquids based on the RFID," *IEEE Trans. Microw. Theory Techn.*, vol. 62, no. 9, pp. 2160–2167, Sep. 2014.

[18] A. P. Gregory and R. N. Clarke, "A review of RF and microwave techniques for dielectric measurements on polar liquids," *IEEE Trans. Dielectr. Electr. Insul.*, vol. 13, no. 4, pp. 727–743, Aug. 2006.

[19] F. Shen *et al.*, "Noncontact measurement of complex permittivity based on the principle of mid-range wireless power transfer," *IEEE Trans. Microw. Theory Techn.*, vol. 62, no. 3, pp. 669–678, Mar. 2014.

[20] J. Baker-Jarvis, M. D. Janezic, P. D. Domich, and R. G. Geyer, "Analysis of an open-ended coaxial probe with lift-off for nondestructive testing," *IEEE Trans. Instrum. Meas.*, vol. 43, no. 5, pp. 711–718, Oct. 1994.

[21] J. Dong, F. Shen, J. Huangfu, S. Qiao, C. Li, and L. Ran, "Non-contact measurement of complex permittivity based on coupled magnetic and electric resonances," in *Proc. IEEE Topical Conf. Biomed. Wireless Technol., Netw., Sens. Syst. (BioWireleSS)*, Jan. 2015, pp. 1–3.

[22] V. Sekar, W. J. Torke, S. Palermo, and K. Entesari, "A self-sustained microwave system for dielectric-constant measurement of lossy organic liquids," *IEEE Trans. Microw. Theory Techn.*, vol. 60, no. 5, pp. 1444–1455, May 2012.

[23] C.-S. Lee and C.-L. Yang, "Thickness and permittivity measurement in multi-layered dielectric structures using complementary split-ring resonators," *IEEE Sensors J.*, vol. 14, no. 3, pp. 695–700, Mar. 2014.

[24] M. S. Boybay and O. M. Ramahi, "Material characterization using complementary split-ring resonators," *IEEE Trans. Instrum. Meas.*, vol. 61, no. 11, pp. 3039–3046, Nov. 2012.

[25] I. Arnedo *et al.*, "Forward and backward leaky wave radiation in split-ring-resonator-based metamaterials," *IET Microw. Antennas Propag.*, vol. 1, no. 1, pp. 65–68, Feb. 2007.

[26] R. Marques, F. Mesa, J. Martel, and F. Medina, "Comparative analysis of edge- and broadside- coupled split ring resonators for metamaterial design—Theory and experiments," *IEEE Trans. Antennas Propag.*, vol. 51, no. 10, pp. 2572–2581, Oct. 2003.

[27] D. M. Pozar, *Microwave Engineering*. Amherst, OH, USA: Wiley, 2005.

[28] B. A. Auld and J. C. Moulder, "Review of advances in quantitative eddy current nondestructive evaluation," *J. Nondestruct. Eval.*, vol. 18, no. 1, pp. 3–36, Mar. 1999.

[29] J. A. Kong, *Electromagnetic Wave Theory*. New York, NY, USA: Wiley, 1986.

[30] *Evaluation of Measurement Data–Guide to the Expression of Uncertainty in Measurement*, document JCGM 100, 2008.

[31] Y. L. Chou, *Statistical Analysis for Business and Economics*. North Holland, The Netherlands: Elsevier, 1989.

[32] R. J. Meredith, *Engineers' Handbook of Industrial Microwave Heating*. London, U.K.: IET, 1998, p. 29.

This article has been accepted for inclusion in a future issue of this journal. Content is final as presented, with the exception of pagination.



[33] M. L. Minges, *Electronic Materials Handbook: Packaging*. Materials Park, OH, USA: ASM International, pp. 599–606, 1989.
[34] A. Khan, *Introduction to Electrical, Electronics and Communication Engineering*. New Delhi, India: Firewall Media, 2005, p. 99.
[35] M. D. Janezic and J. A. Jargon, "Complex permittivity determination from propagation constant measurements," *IEEE Microw. Guided Wave Lett.*, vol. 9, no. 2, pp. 76–78, Feb. 1999.

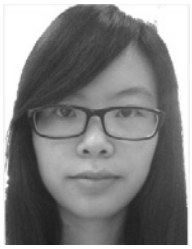

**Jing Dong** received the bachelor's and master's degrees from Zhejiang University, Hangzhou, China, in 2012 and 2015, respectively.

She was with the Laboratory of Applied Research on Electromagnetics, Zhejiang University. She is currently involved in science and technology with the Electromagnetic Compatibility Laboratory, China Ship Development and Design Center, Wuhan, China. Her current research interests include the measurement and imaging of material property.

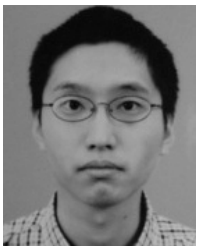

**Fazhong Shen** received the B.S. and Ph.D. degrees from Zhejiang University, Hangzhou, China, in 2008 and 2013, respectively.

He has been with the China Research Institute of Radiowave Propagation, Xinxiang, China, since 2014. His current research interests include the measurement and imaging of material property and wireless power transfer.

**Yazhou Dong** received the B.S. degree from Xi'an Jiaotong University, Xi'an, China, in 2006, and the M.S. degree from Southeast University, Nanjing, China, in 2009.

He is currently a Microwave Engineer with the National Key Laboratory of Science and Technology on Space Microwave, China Academy of Space Technology, Xi'an, China. His current research interests include space microwave technologies powered by microwave power transmission, microwave power combining, and antenna array technology.

**Ying Wang** received the B.S. degree from Northwestern Polytechnical University, Xi'an, China, in 2004, and the M.S. degree from the China Academy of Space Technology, Xi'an, China, in 2007.

She is currently with the National Key Laboratory of Science and Technology on Space Microwave, Xi'an, China. Her current research interests include solid-state power device and microwave power transmission.

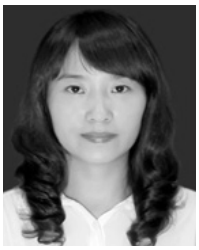

**Wenli Fu** received the bachelor's and master's degrees in electromagnetics and microwave technology from the University of Electronic Science and Technology of China, Chengdu, China, in 2010 and 2013, respectively.

She is currently with the National Key Laboratory of Science and Technology on Space Microwave, Xi'an, China. Her current research interests include high-efficiency power amplifier and rectenna design and microwave power transmission systems.

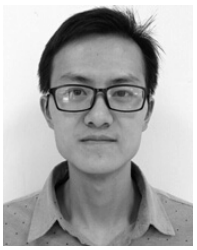

**Huan Li** received the B.S. degree from Xidian University, Xi'an, China, in 2011. He is currently pursuing the Ph.D. degree with the Laboratory of Applied Research on Electromagnetics, Zhejiang University, Hangzhou, China.

His current research interests include microwave circuits, antennas, measurement, and artificial metamaterials.

**Dexin Ye** received the B.S. and Ph.D. degrees in electrical engineering from Zhejiang University, Hangzhou, China, in 2007 and 2013, respectively.

He visited the University of Arizona, Tucson, AZ, USA, for six months, and the Massachusetts Institute of Technology, Cambridge, MA, USA, for one year from 2011 to 2013 as a Visiting Ph.D. Student. He is currently with the Laboratory of Applied Research on Electromagnetics, Zhejiang University. His current research interests include artificial active metamaterials, perfectly matched layers, and radio-frequency and microwave applications.

**Bin Zhang** received the B.S. degree in electrical engineering from the Vocational and Technological Education Center, Huzhou, China, in 2004.

He is currently an Experimental Engineer with the Laboratory of Applied Research on Electromagnetics, Zhejiang University, Hangzhou, China.

**Jiangtao Huangfu** received the B.S. and Ph.D. degrees in electrical engineering from Zhejiang University, Hangzhou, China, in 1999 and 2004, respectively.

He became a Lecturer with the Department of Information and Electronic Engineering, Zhejiang University, in 2004, where he has served as an Associate Professor since 2006. He was a Visiting Scientist with the Massachusetts Institute of Technology, Cambridge, MA, USA, in 2007, and the California Institute of Technology, Pasadena, CA, USA, in 2013 and 2014. He is currently with the Laboratory of Applied Research on Electromagnetics, Zhejiang University. His current research interests include RF and microwave circuits, antennas, and microwave metamaterials.

**Shan Qiao**, photograph and biography not available at the time of publication.

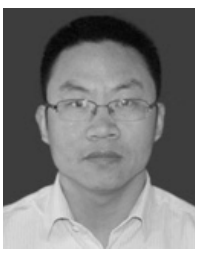

**Yongzhi Sun** received the Ph.D. degree from the State Key Laboratory of Millimeter Wave, Southeast University, Nanjing, China.

He is currently the Team Leader of the Antenna Division with the Nanjing Institute of Electronic Equipment, Nanjing, China. His current research interests include new concept antenna systems, radio-frequency and microwave devices, and microwave absorbing materials.

Dr. Sun was a recipient of multiple government awards from the Program for the Top Young Innovative Talents, the 333 Project of Jiangsu Province, and the China Soong Ching Ling Foundation.

This article has been accepted for inclusion in a future issue of this journal. Content is final as presented, with the exception of pagination.



**Changzhi Li** (S'06–M'09–SM'13) received the B.S. degree in electrical engineering from Zhejiang University, Hangzhou, China, in 2004, and the Ph.D. degree in electrical engineering from the University of Florida, Gainesville, FL, USA, in 2009.

He was with Alereon Inc., Austin, TX, USA, and Coherent Logix Inc., Austin, TX, from 2007 to 2009, where he was involved in ultra-wideband transceivers and software-defined radio. He joined Texas Tech University, Lubbock, TX, USA, as an Assistant Professor in 2009, where he became an Associate Professor in 2014. His current research interests include biomedical applications of microwave/RF, wireless sensor, and analog circuits.

Dr. Li was the recipient of the ASEE Frederick Emmons Terman Award in 2014, the IEEE-HKN Outstanding Young Professional Award in 2014, the NSF Faculty Early CAREER Award in 2013, and the IEEE MTT-S Graduate Fellowship Award in 2008. He was the recipient of nine Best Conference/Student Paper Awards as an author/advisor in IEEE-sponsored conferences. He is an Associate Editor of the IEEE TRANSACTIONS ON CIRCUITS AND SYSTEMS—II: EXPRESS BRIEFS. He served as the TPC Co-Chair of the IEEE Wireless and Microwave Technology Conference in 2012 and 2013.

**Lixin Ran** received the B.S., M.S., and Ph.D. degrees from Zhejiang University, Hangzhou, China, in 1991, 1994, and 1997, respectively.

He became an Assistant Professor in 1997, an Associate Professor in 1999, and a Full Professor in 2004 with the Department of Information and Electronics Engineering, Zhejiang University. He visited the Massachusetts Institute of Technology, Cambridge, MA, USA, as a Visiting Scientist in 2005, 2009, and 2012. He is currently the Director of the Laboratory of Applied Research on Electromagnetics, Zhejiang University. He has co-authored over 130 research papers published in peer-reviewed journals and holds over 30 licensed patents. His current research interests include new concept antennas, radio-aware sensing and imaging, radio frequency, microwave and terahertz systems, and artificial active media.

View publication stats